ACS Catalysis

Research Article

pubs.acs.org/acscatalysis

Electrochemical Hydrogen Production in Acidic Water by an Azadithiolate Bridged Synthetic Hydrogenese Mimic: Role of Aqueous Solvation in Lowering Overpotential

Subal Dey, Atanu Rana, Somdatta Ghosh Dey,* and Abhishek Dey*

Department of Inorganic Chemistry, Indian Association for the Cultivation of Science, Kolkata, India 700032

Supporting Information

ABSTRACT: An inherent problem stalling the development of a H_2-based global energy economy is the unavailability of efficient functional catalysts that can function in aqueous media. A Fe−Fe hydrogenase mimic is investigated for electrocatalytic hydrogen generation in aqueous medium. H_2 is produced from acid water (pH <3) by a Fe−Fe hydrogenase mimic immobilized on graphite surfaces. These catalysts are known to reduce H^+ at very negative potentials in organic solvents. However, in aqueous medium, the H^+ reduction potential is shifted to much more positive values. The catalyst shows a turnover frequency of 6400 s^{-1} at −0.5 V and an onset potential of −0.36 V vs NHE. Prolonged electrolysis shows that the catalyst has a turnover number $\gg 10^8$ and a Faradaic efficiency > 95%. Even at pH 2, that is, $[H]^+$ = 0.01 N, $I_{cat}/[\tau]$ > 400 s^{-1} is obtained. The catalyst can be immobilized on cheap carbon electrodes, used in domestic Zn-Carbon dry batteries, to generate H_2 from acid aqueous solutions.

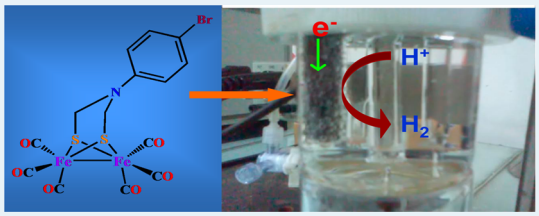

KEYWORDS: *hydrogen evolution reaction, iron hydrogenase, bio-inspired catalysis*

INTRODUCTION

The ever increasing global energy demand and depleting fossil fuel sources have instigated great interest in the development of clean and sustainable alternate energy sources.[1,2] Additionally, because of increasing concerns regarding the ecological/environmental consequences of accumulating vast amounts of CO_2 in the atmosphere, as a result of the relentless use of fossil fuels as the chief sources of energy for centuries, a carbon neutral energy source is of global interest.[3−5] A H_2 based energy economy heralds such potential,[6,7] but its success demands the availability of efficient, durable, and inexpensive metal catalysts that can catalyze H_2 production at minimum overpotentials with high turnover rates.[8−11] Although Pt is suitable for this purpose, its scarcity and consequently its price has led to a global search for alternative transition metal based catalysts.[12] Over the past decade elegant Mn,[13] Ni,[14−18] and Co[19−27]-based organometallic molecular complexes have been evaluated for catalytic/electrocatalytic H^+ reduction. Most of these are found to be limited by their instability/insolubility in aqueous environment, requirement of high overpotential, and low turnover rates.[28−33] A few Co or Ni-based electrocatalysts are reported which exhibit high turnover frequencies either in organic media or in aqueous media. Very recently, efficient Mo-based molecular electrocatalysts have been reported to catalyze H^+ reduction in aqueous medium.[34,35] Some of these catalysts demand large overpotentials to generate hydrogen at detectable rates. An efficient Fe-based molecular electrocatalyst is desirable as iron is the most abundant transition metal in the lithosphere (∼1000 times more abundant than Co) and ∼2.6 billion tones of it is produced annually worldwide which is higher than any other transition metals (copper comes second in the list with an annual production of 16 million tones).[10,36−38] However, very few Fe-complexes are known to produce H_2 via H^+ reduction in the aqueous medium.[39]

Hydrogenase (H_2ase) enzymes reversibly converts protons to hydrogen with minimum over potential at physiological pHs with turnover frequency (TOF) of 100 to 10,000 mols of H_2 per mole of enzyme per second.[40,41] There are three types of H_2ase, namely, binuclear Ni−Fe H_2ase, binuclear Fe−Fe H_2ase, and mononuclear Fe-only H_2ase, which are abundant in nature.[42,43] The Fe−Fe H_2ase mainly reduces protons to H_2 whereas the Ni−Fe H_2ase is known for H_2 oxidation while the Fe-only H_2ase is not catalytic by itself.[41] These are very sensitive to oxygen and loose their catalytic activity permanently.[44] The Fe−Fe H_2ase active site contains a $Fe_2S_2(CO)_3(CN)_2$ organometallic core (Figure 1A).[45] A bismethylene azadithiolate (ADT) moiety bridges between the two Fe centers.[43,46] Numerous synthetic structural and some functional H_2ase models with a basic $Fe_2S_2(CO)_6$ core are known, and their catalytic hydrogen generation in organic solvents are reported.[46,47] However these investigations, exclusively performed in nonaqueous solvents and in homogeneous conditions reveal that they require very low potential and show limited TOF.[48] The low over potential is due to the fact that these catalysts, isolated in their Fe(I)Fe(I) neutral forms, have to be reduced to the dianionic Fe(0)Fe(0)

Received: July 30, 2012
Revised: January 22, 2013

   dx.doi.org/10.1021/cs300835a | ACS Catal. 2013, 3, 429−436

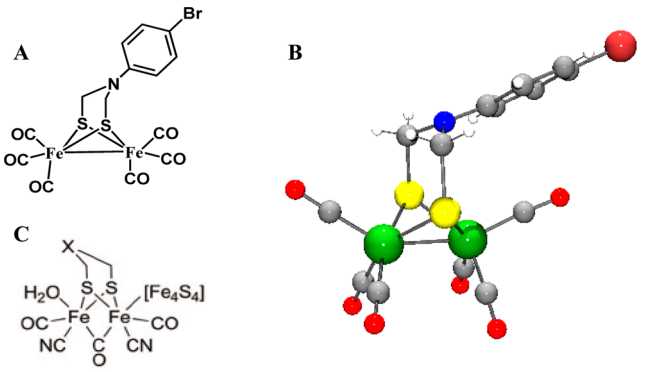

Figure 1. (A) Schematic diagram of complex **A**, (B) X-ray crystallographically determined structure of complex **A**, and (C) the active site of Fe−Fe hydrogenase.

state for catalysis in nonaqueous medium. Recent studies in homogeneous hydrogen evolution by a micellar H_2-ase mimic by photochemical and electrochemical means in aqueous media provided the information to achieve the high TOF.[36,49]

Here, we report, for the first time, heterogeneous electrochemical H_2 production by reducing protons in acidic aqueous media by a robust synthetic Fe−Fe H_2-ase active site mimic having a $Fe_2S_2(CO)_6$ core (Figure 1B, complex **A**) and a bridging ADT ligand. The catalytic property of this catalyst in aqueous medium is investigated using RDE, RRDE coulometry, and bulk electrolysis technique.

RESULTS AND DISCUSSION

X-ray Photoelectron Spectroscopy (XPS) of Complex A Immobilized on Electrodes. XPS analysis of the electrode bearing complex **A** show the presence of Fe (Figure 2A), S (Figure 2B), N (Figure 2C), C (Figure 2D) and Br (Figure 2E) on the electrode surface. The Fe_{2p} ionizations were observed at 711.1 eV ($2p_{1/2}$) and 724.5 eV ($2p_{3/2}$) consistent with data obtained on similar complexes.[50] The binding energies of the N (1s) and S (2p) are at 399.3 and 161.9 eV which is consistent with those observed for tertiary aromatic amines and metal thiolate complexes.[51−53] In addition to the major peak observed for graphite (285.5 eV, Figure 2D, dashed red), the C1s region also shows a peak at 286.8 eV (Figure 2D, dashed blue), characteristic of carbonyl group. These data are consistent with the presence of complex **A** on the electrode.

Cyclic Voltammetry (CV). The CV of complex **A** in acetonitile shows two well established quasi-reversible one electron reductions ($E_{1/2}$) at −0.61 V and −0.89 V corresponding to the Fe^I-Fe^I/Fe^I-Fe^0 and Fe^I-Fe^0/Fe^0-Fe^0 redox couples (Figure 3, orange) consistent with a previous report.[54] The first wave at −0.61 V has a peak to peak separation (ΔE_p) of 136 mV, and the second wave at −0.89 V has a ΔE_p of 140 mV. The cyclic voltammogram of complex **A** physisorbed on the EPG electrode in water shows two reversible waves centered at −0.22 V and −0.37 V for the Fe^I-Fe^I/Fe^I-Fe^0 and Fe^I-Fe^0/Fe^0-Fe^0 redox couples (Figure 3, blue). Integration of the charge under these processes yields the total number of electroactive complex **A** species on the electrode to be ~10^{-11} moles.[55,56] The CV current increases linearly with increase in scan speed consistent with the presence of adsorbed species on the electrode (Supporting Information, Figure SI−II). The ΔE_p for the two consecutive reduction waves are 200 mV and 240 mV, respectively. Thus the Fe^I-Fe^I/Fe^I-Fe^0 and Fe^I-Fe^0/Fe^0-Fe^0 reduction potentials shift by +0.38 and +0.52 V on changing the solvent from CH_3CN to H_2O.

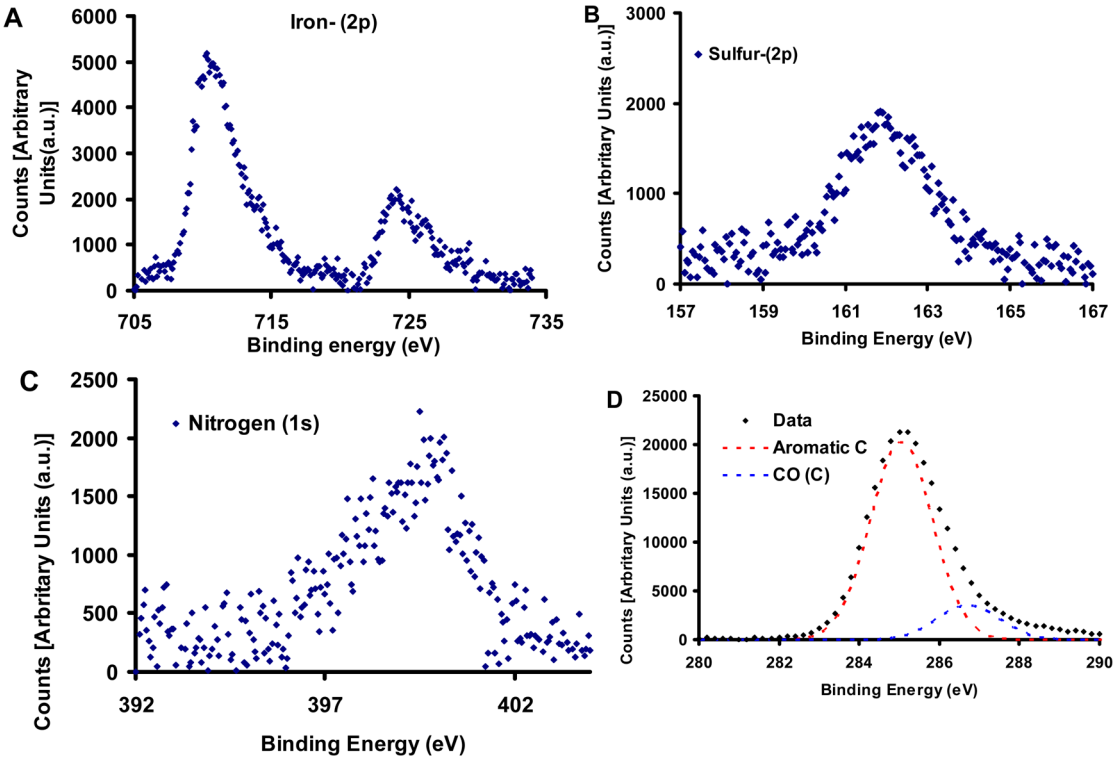

Figure 2. XPS study of the complex **A**, adsorbed on the EPG electrode. (A) Spectra of Iron-2p core level. (B) Spectra for Sulfur-2p core level. (C) Spectra of Nitrogen-1s core level. (D) Spectra of Carbon-1s core level. Corresponding peak-fitted spectra have been overlapped with the experimentally obtained spectra.

dx.doi.org/10.1021/cs300835a | ACS Catal. 2013, 3, 429−436

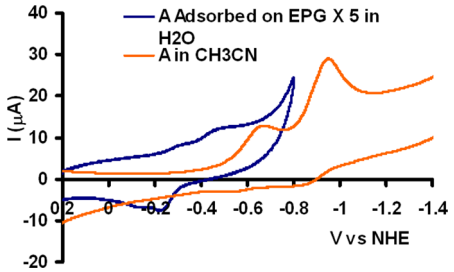

Figure 3. CV of a solution of complex **A** in acetonitrile/$(nBu)_4NClO_4$ (orange) with a glassy carbon working electrode and CV of complex **A** immobilized on the EPG electrode in H_2O/KPF_6 (blue). Data was obtained at a scan rate of 200 mV/s using a Pt counter electrode and an aqueous Ag/AgCl reference and converted to NHE reference.

The positive shift in $E_{1/2}$ in a polar aqueous medium is possibly due to the enhanced stability of the reduced anionic species (A^- or A^{2-}) in polar water medium relative to the neutral oxidized complex (A).[57] The increased solvation of the reduced anionic species stabilizes it more relative to the neutral oxidized species making these complexes easier to reduce, that is, more positive reduction potential. The reduction of A^- to A^{2-} shows a greater shift relative to A to A^- because of greater negative charge on the A^{2-} species. Geometry optimized density functional theory (DFT) calculations (on this complex) indicate that the calculated formal potential for the two electron reduction of Fe(I)Fe(I) to Fe(0)Fe(0) shifts 475 mV positive in H_2O relative to CH_3CN (solvation modeled using PCM) consistent with the positive shifts observed experimentally. The large positive shifts observed in the reduction potential in aqueous medium encouraged us to investigate the electrocatalytic behavior of **A** in aqueous medium in the presence of a cheap proton source.

Electrocatalytic H^+ Reduction. *(a). Rotating Ring Disc Electrochemistry (RRDE).* In a linear sweep voltammetry (LSV) scan of the complex **A** immobilized on the EPG electrode immersed in 0.01 N H_2SO_4 solution (pH 2) a large electrocatalytic current (Figure 3, blue) is observed as the potential of the working electrode is lowered. Almost no catalytic current is observed if the catalyst is not immobilized on the electrode (Figure 4, green line). Concomitant bubble formation is observed on the electrode surface suggesting the formation of H_2 gas. The production of H_2 is confirmed by

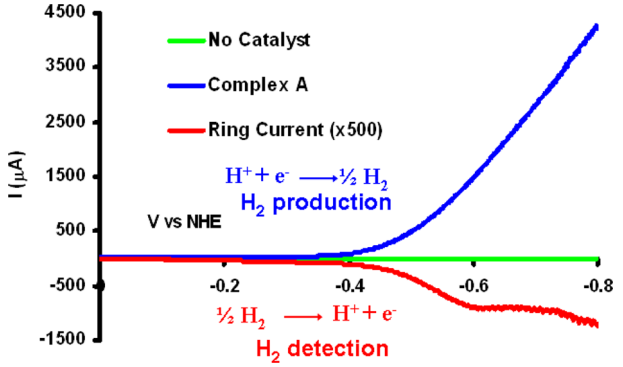

Figure 4. RRDE with complex **A** on the EPG disc working electrode (blue line, indicating H_2 generation) which is swept from 0.2 V to −0.8 V and the corresponding Pt-ring current (red line, indicating H_2 detection) with the ring held at a constant potential of 0.7 V in aqueous 0.01 N H_2SO_4.

oxidizing it back to H^+ on a Pt ring which encircles the working electrode when held at a *constant* potential of 0.7 V (at this potential Pt oxidized H_2 to H^+) as described previously.[16] In an RRDE setup the H_2, produced at the EPG electrode (Figure 4, blue line) and diffused toward the Pt ring because of the hydrodynamic flow created by the rotating shaft, gets oxidized to H^+, and an oxidation current is recorded at the ring (Figure 4, red line).[16] Note that unlike RRDE of dissolved species, where ∼20% of the product can be detected on the Pt ring, only 1−1.5% of the hydrogen produced in the working electrode is detected on the ring as hydrogen, being an insoluble gas, escapes readily from the solution (see Experimental Details section).[16] The RRDE data clearly show that the H_2 oxidation current at the Pt ring is observed only where H^+ reduction current is observed at the working electrode bearing complex **A**, that is, at $E < -0.4$ V. The onset potential for H^+ reduction (the potential where at least 50 μA of H^+ reduction current is observed at the working electrode and the corresponding H_2 formed can be detected on the Pt ring) of complex **A** in 0.05 N H_2SO_4 solution is −0.36 V.[58] The thermodynamic proton reduction potential at pH 3 is −0.18 V vs NHE. Thus complex **A** requires an overpotential of only 180 mV to be functional in aqueous solutions. Note that it has been recently shown that the overpotential can be related to the intrinsic TON and TOF of an electrocatalyst.[59,60] This "foot-of-the-wave" analysis can also be used in this case to obtain the kinetic parameters (vide-infra).

(b). $[H]^+$ Dependence. H^+ reduction is investigated over a large range of proton concentration of 0.001−0.5 N (i.e., pH 3−0.3) by rotating disk electrochemistry (RDE). With increasing acid concentrations the electrocatalytic hydrogen production rate increases gradually till it saturates at 0.5 N (Figure 5A). No further enhancement of catalytic current is observed on increasing the H^+ concentration. The nature of the catalytic current suggests that it is not substrate diffusion limited as is the case for most O_2 reduction electrocatalysts which are immobilized on EPG electrodes. Substrate diffusion limited catalytic current is independent of the potential applied on the working electrode. This is not the case here. Thus a normal Koutecky−Levitch analysis could not be performed to obtain the k_{cat}. However the intrinsic second order rate (k_{cat}) of the catalyst could be determined from the foot of the wave analysis of the LSV data obtained in 0.5 N H_2SO_4 solution, as described in the Supporting Information. However, the ratio of the catalytic current (I_{cat}, converted to moles of H_2 produced per second) and the number of moles of electroactive complex **A** present in the electrode ($[\tau]$, obtained from the integration of the CV current) can be used as a measure of catalytic efficiency ($I_{cat}/[\tau]$, this has an unit of s^{-1}). The catalytic efficiency is estimated to be 6400 s^{-1} in 0.5 N H_2SO_4 at −0.5 V, that is, 6400 mols of electrons are dissipated from the electrode per second per mole of the catalyst. Consecutive RDE scans (up to 200 scans) in 0.5 N H_2SO_4 show no noticeable decrease in the catalytic current (Figure 5B). This implies that the catalyst is quite stable under the experimental conditions. Note that even at $[H]^+ < 0.01$, that is, at pH 2, $I_{cat}/[\tau] > 400$ s^{-1} is detected (Figure 5A, inset).

An overlay of the CV data in the absence of $[H^+]$ with the LVS data in the presence of increasing amount of H^+ (Figure 6) reveals that the potential at which H^+ reduction starts varies with $[H]^+$ such that the H^+ reduction occurs at much lower potentials at lower $[H^+]$. This implies that the catalytic mechanism is $[H]^+$ dependent, and at lower $[H]^+$ higher

dx.doi.org/10.1021/cs300835a | ACS Catal. 2013, 3, 429−436

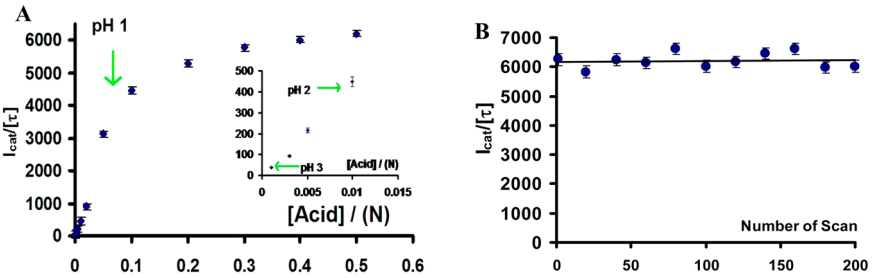

Figure 5. (A) Plot of $I_{cat}/[\tau]$ at varying acid concentrations. I_{cat} values were recorded at −0.5 V vs NHE at each acid concentration. (B) Plot of $I_{cat}/[\tau]$ vs number of scan (N).

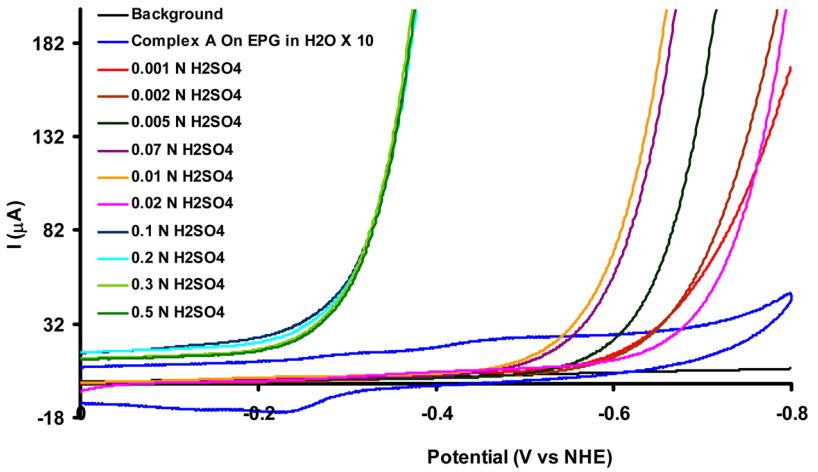

Figure 6. RDE for electrochemical hydrogen generation with increasing acid concentration (Current vs Potential). (A) Catalytic current for low acid concentrations (0.001 N−0.5 N H_2SO_4). Data were obtained using a Pt-counter electrode, referred to an NHE reference electrode and complex **A** adsorbed EPG working electrode and H_2O-KPF_6 electrolyte. H_2SO_4 was added externally.

driving forces are required to obtain measurable rates of H^+ reduction. At $[H]^+ > 0.1$ N the electrocatalytic current coincides with the reduction of the complex to its mixed valent Fe(I)Fe(0) state. Thus the Fe(I)Fe(0) state is the active form of the catalyst at these acid concentrations. However at $[H]^+ < 0.02$ N, the H^+ reduction coincides with the reduction of the cluster to its Fe(0)Fe(0) state (Figure 6). Thus at these acid concentrations the Fe(0)Fe(0) state is active. This may reflect the relative pK_a's of the Fe(I)Fe(0) and the Fe(0)Fe(0) states (assuming that the H^+ reduction occurs via protonation of the catalyst). The former has lesser electron density than the latter, and hence its protonation may occur at higher acid concentrations than the latter.

Controlled Potential Coulometry (Bulk Electrolysis). For estimating the Faradaic efficiency of the catalyst A, controlled potential coulometry (CPE) is performed at 0.5 N H_2SO_4 for a period of 8 h at −0.5 V in a two compartment cell. In these experiments consumption of 1.10×10^2 C charge (i.e., $1.10 \times 10^2/F = \sim 1.14 \times 10^{-3}$ moles of electrons) from the electrode (Figure 7, red) was recorded. A bare EPG electrode dissipated only 0.14 C charge when held at −0.5 V (Figure 7, green). The H_2 gas formed in the process was trapped in an inverted burette setup and was measured to be 12 mL at 1 atm. This yields a Faradaic yield (FY) of 94% (12.8 mL = 100% FY).

To ensure the integrity of the complex of the electrode, FTIR data as well as XPS data are collected before and after the electrolysis experiments. The IR spectrum of the catalyst A has been recorded after grafting it onto the EPG (Figure 8, blue). After continuous electrolysis at −0.5 V in 0.5 N H_2SO_4 solution the FTIR spectrum is recorded again (Figure 8, red). The data

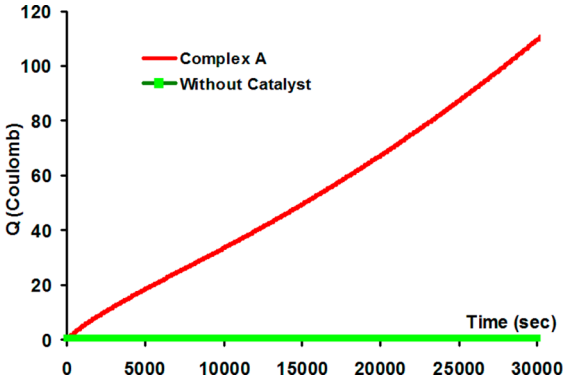

Figure 7. Controlled potential bulk electrolysis voltamogram at −0.5 V vs NHE in aqueous 0.5 N H_2SO_4. The red line indicates the charge accumulated by the catalyst absorbed electrode, and the green line represents the charge accumulated without catalyst.

show minimum changes in energies and relative intensities of the vibrations observed in the CO and C−H stretching regions. Similarly very little change in the relative intensity of the XPS spectra is detected (Supporting Information, Figure SI−IV). Thus the catalyst retains its integrity during the electrolysis process. This is different from the results obtained on HOPG and Au electrodes covalently modified with similar catalysts where rapid degradation of these catalysts was observed. A key difference between these experiments and the one performed before is the reaction medium. While here acidic aqueous medium is used, in all of the above cases CH_3CN was used as

dx.doi.org/10.1021/cs300835a | *ACS Catal.* 2013, 3, 429−436

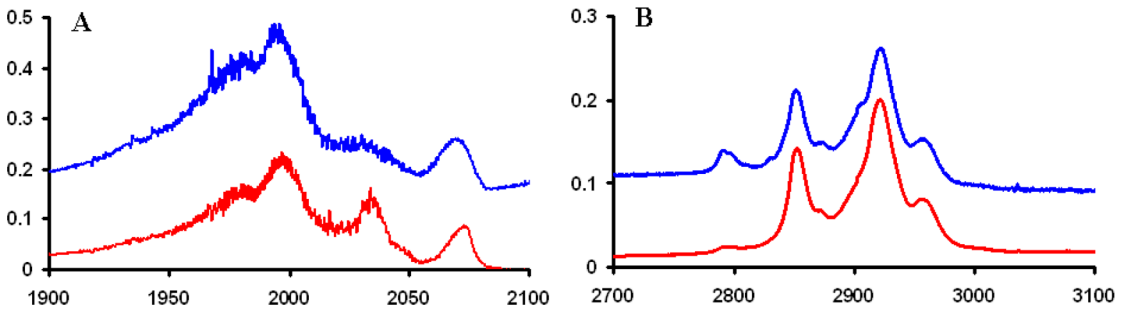

Figure 8. IR spectra of the catalyst A onto the EPG surface before (blue) and after electrolysis (red). (A) C−O vibration region; (B) C−H vibration region. (*X*-axis in cm^{-1}).

the solvent and HBF_4 or some other organic acid was used as the proton donor.[50] These catalysts, once immobilized on graphite surfaces, seem to be more stable in acidic aqueous medium relative to acidic organic medium.

Turnover Frequency (TOF) and Turnover Number (TON). The CV experiments indicate that there are $\sim 10^{-11}$ moles of catalyst immobilized on the EPG electrode which could be obtained by integration of the current density under the oxidation and reduction waves. The controlled potential electrolysis experiments at −0.5 V indicate that $\sim 1.1 \times 10^{-3}$ moles of H^+ is reduced without any decay in the catalytic activity in 8 h. Thus, the TON for the catalyst can be estimated to be $\gg 10^8$. The TOF determined from the $I_{cat}/[\tau]$ ratio is 6400 s^{-1} in 0.5 N H_2SO_4. Alternatively, during bulk electrolysis 1.1×10^{-3} turnovers were detected in 8 h by 10^{-11} moles of catalyst. The average TOF during the bulk electrolysis experiment is estimated to be $\sim 6 \times 10^3$ s^{-1} (10^8 turnovers over 8 h = ∼6000 turnovers per second) at −0.5 V in 0.5 N H_2SO_4, which is comparable to the value obtained from LSV. A foot of the wave analysis (Supporting Information, Figure SI−VI) of the LSV data has been performed to determine the intrinsic second order rate (k_{cat}) of this catalyst to be ∼33000 M^{-1} s^{-1}.[59,60] A plot of log(TOF) and overpotential (η) obtained from this analysis agrees reasonably well with the estimate obtained from bulk electrolysis experiments. Considering the fact that $\sim 10^{-11}$ moles of complex **A** produce 12 mL, that is, 0.6×10^{-3} moles of hydrogen over a period of 8 h in 0.5 N H_2SO_4 at −0.5 V, one can estimate the yield of H_2 per mole of the catalyst to be $\sim 4.4 \times 10^4$ liter/sec per mole of complex **A**. This is equivalent to ∼83 L/sec/gram of catalyst. To the best of our knowledge this is possibly the highest electrocatalytic H_2 generation rate reported so far[34,36,61] and is comparable to the highest activity reported for the native enzymes.

H_2 Generation from Domestic Carbon Electrodes. Encouraged by the bulk electrolysis results on EPG electrodes, H_2 production was also investigated by adsorbing the catalyst on the surface of very cheap carbon electrodes conventionally used in domestic 1.5 V Zinc−Carbon dry batteries. Profuse evolution of H_2 gas was observed on the cathode (Figure 9, also see Supporting Information video) and in parallel O_2 gas liberation was observed in the Pt mesh cathode when a potential of −0.5 V was applied to the working electrode. Thus complex **A** can in fact be immobilized even on very cheap electrodes to generate H_2 from acidic water at −0.5 V vs NHE.

CONCLUSION AND COMMENT

In summary, we report, for the first time, H_2 formation from acidic H_2O (pH < 3) by a synthetic mimic of FeFe H_2ase bearing an ADT bridge. Enhanced solvation of the active species (i.e., the reduced complex **A**) in an aqueous medium raises the thermodynamic reduction potential which allows H_2 production from H_2O at reasonable potentials. FTIR data of the catalyst, immobilized on the electrode, before and after the electrocatalytic processes indicates that the complex is quite stable under these conditions. The onset potential, TON, and TOF obtained, when compared to that of other catalysts reported in the literature (Table 1), suggests that this is an excellent electrocatalyst for H_2 generation. While some Mo based catalysts show reasonable H_2 generation at pH 7, this Fe based catalyst has superior TOF and low overpotential. This catalyst has the highest TON ($\gg 10^8$) and TOF in aqueous medium of all the catalysts reported to date (Table 1). In addition to that, its reactivity is retained when immobilized on cheap carbon electrodes, which is of significant practical interest.

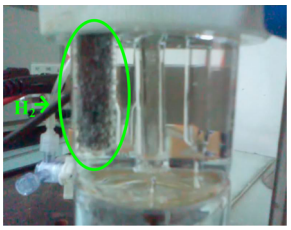

Figure 9. Control Potential Coulometry at −0.5 V vs NHE showing electrochemical H_2 generation from 0.5 N H_2SO_4 using a cheap graphite electrode.

EXPERIMENTAL DETAILS

General Procedures. Compound **A** was synthesized using the standard Schlenk technique. Anaerobic experiments were performed within an MBRAUN glovebox. The solvents used were purchased from Merck Specialties, Pvt. Ltd. (India), Spectrochem Pvt. Ltd. (India), RFCL Ltd. (India), Avra synthesis Pvt. Ltd. (India). *p*-Bromoaniline and thionyl chloride ($SOCl_2$) were purchased from Spectrochem Pvt. Ltd. (India), *p*-formaldehyde and superhydride ($LiBEt_3H$, 1 M in THF) were bought from Sigma-Aldrich chemicals Pvt. Ltd., and anhydrous Na_2SO_4 and sulfuric acid (98%) were purchased from Merck Specialties, Pvt. Ltd. (India). SiO_2 (60−120) was purchased from SISCO Pvt. Ltd. (India). Triple distilled deionized water has been used for all electrochemical experiments. Column chromatography was performed on SiO_2 (60−100 mesh). Edge Plane Graphite (EPG) discs were purchased from Pine Instruments. The FT-IR data are measured on the Shimadzu FTIR 8400S instrument. All the NMR spectra were recorded on the Bruker DPX-300 or DPX-500 spectrometer at room temperature. The mass spectra are

dx.doi.org/10.1021/cs300835a | *ACS Catal.* 2013, 3, 429−436

Table 1. Comparison of H_2 Evolving Electrocatalysts

catalyst	onset E (V) Vs NHE	pH	performance		ref
			TON[a]	TOF[b]	
Co nanoparticle	−0.65 V	pH 7			26
Co pentapyridine	−1.07 V	pH 7	$\sim 10^4$	0.35 s^{-1}	27
MoS_2 catalyst	−0.65 V	pH 3	$\sim 10^3$	280 s^{-1}	35
Mo Oxo catalyst	−0.93 V	pH 7	$\sim 10^5$	2.4 s^{-1}	34
Co tetraaza macrocycle	−0.40 V	pH 2.2	23		25
Co tetraimine catalyst	−0.40 V	pH 2	$\sim 10^{5-6}$		56
Co bis iminopyridine	−0.90 V	pH 2		2.2 h^{-1}	33
$Fe_2S_2Ph(CO)_6$-SDS surfactant	>−0.7 V	pH 3	52	2600 s^{-1}	36
complex **A**	−0.3 V	pH 2−1	$\gg 10^8$	6400 s^{-1} k_{cat} $\sim 3.3 \times 10^4$ M^{-1} s^{-1}	this work

[a]Moles of H_2 per mole of catalyst. [b]Generally calculated at 100−300 mV below the onset potential.

recorded by a QTOF Micro YA263 instrument. X-ray single crystal data was collected at 120 K using radiation on a SMART APEX diffractometer equipped with CCD area detector. Data collection, data reduction, and structure solution refinement were carried out using the software package of APEX II. The structure was solved by the direct method and refined in a routine manner. The nonhydrogen atoms were treated anisotropically. All the hydrogen atoms were located on a difference Fourier map and refined.

Synthetic Procedure for Complex A, $BrC_6H_4N(CH_2S)_2Fe_2(CO)_6$. Complex **A** was synthesized according to the literature procedure using a standard Schlenk technique.[54] $Fe_2S_2(CO)_6$[54,62](438 mg, 1 mmol) was dissolved in 20 mL of dry tetrahydrofuran (THF). Two milliliters of $LiBEt_3H$ (1 M in THF) was added dropwise to the red solution at −78 °C. The solution immediately turned to deep green. The ligand *p*-$BrC_6H_4N(CH_2)_2Cl_2$, synthesized by reacting with *p*-$BrC_6H_4NH_2$, *p*-formaldehyde, and thionyl chloride,[62] was added to the reaction mixture at −15 °C. The color immediately changed to dark red. The reaction mixture was stirred for further 1 h at room temperature. Removal of the solvent produces a dark brown precipitate. A crystalline red solid product was obtained after column chromatography with hexane-toluene (4:1) mixture. Single crystal was grown by slow diffusion of the hexane in toluene.

^1H NMR ($CDCl_3$): 7.50−6.52 (4H, dd), 4.27 (s, 4H); IR (CH_3CN): 2074 cm^{-1}(s), 2038 cm^{-1}(s), 2000 cm^{-1}(s); ESI^+ Mass(TOF) $[M + H]^+$ = 540.3941; Calculated $[m/z]$ = 539.772.

ATR-FTIR Spectroscopy. FT-IR spectra of the Complex **A** adsorbed EPG surface was recorded by a Perkin-Elmer Frontier FT-IR spectrometer. A total of 3000 scans were collected at room temperature before and after electrolysis using the EPG disc electrode.

X-ray Photoelectron Spectroscopy. XPS (XPS, Omicron, model: 1712-62-11) measurement was done using a high resolution monochromatic Mg−Kα radiation source at 1253.6 eV under 15 kV voltage and 5 mA current condition.

Electrochemical Measurements. *Cyclic Voltammetry.* The cyclic voltammograms are recorded on a CH Instrument bipotentiostat model 720D. A glassy carbon electrode and a Pt wire is used as the working and the counter electrode, respectively. The measurements were made against an aqueous Ag/AgCl reference electrode and corrected to NHE. CV experiment on a 1 mM solution of complex **A** and 0.1 N n-Bu_4ClO_4 in acetonitrile was performed in a Glove Box at room temperature. The working glassy carbon electrode was washed and polished before use.

The aqueous aqueous cyclic voltamogram was recorded with the same instrument and same software in 0.1 M KPF_6- water solution with the complex **A** adsorbed EPG discs (5 mm outer diameter) held within a shaft (Pine Instruments, AFE6MB). An anaerobic environment was maintained within a water jacketed electrochemical cell (Pine Instrument, RRPG138) by purging with Ar gas for 1 h. The aqueous Ag/AgCl reference (Pine instruments, RREF0021) and Pt counter (AFCTR5) electrodes were attached to the cell through airtight joints. All potentials reported here are versus aqueous NHE (in saturated KCl) reference electrode.

Construction of Graphite Electrodes with Compound A ($Fe_2S_2(CH2)_2NC_6H_4Br$). *On Edge Plane Graphite (EPG).* A 50 μL portion of a dilute solution (~10 mM, in CH_2Cl_2) is uniformly distributed on a freshly polished EPG disc (5 mm outer diameter). After the CH_2Cl_2 has evaporated, the surface is washed with $CHCl_3$ thoroughly and sonicated in ethanol to remove any loosely bound catalyst on the EPG surface and washed with triple distilled water.

Rotating Disc Electrochemistry. The RDE/RRDE measurements are performed on a CHI 700D bipotentiostat. An EPG disc is used as the working electrode which is mounted inside of a Pt ring assembly (Pine Instrument, AFE6RIP) which is mounted at the tip of a shaft (Pine Instruments, AFE6MB) which in turn is fitted to a MRS rotator. A water jacketed electrochemical cell (Pine Instrument, RRPG138) is obtained where the rotor was inserted through a taper plug assembly (AC01TPA6M) which allows free rotation of the vertical rotor while maintaining an airtight seal. An aqueous Ag/AgCl reference (Pine instruments, RREF0021) and Pt counter (AFCTR5) electrodes are attached to the cell through airtight joints. The graphite surface is cleaned by polishing it uniformly on a Silicon carbide grinding paper followed by sonication in triple distilled water. The complex is then physisorbed on the disc as described above.

Electrochemical Hydrogen Production by Complex A Adsorbed on EPG in Aqueous H_2SO_4. The shaft bearing the EPG electrode and the Pt ring is vertically inserted to the water jacket cell, and the cell is purged with N_2 for 30−60 min. Hydrogen generation experiments have been investigated in thoroughly degassed solutions (free-pump-thaw) to eliminate any electrocatalytic O_2 reduction. Background scans are performed under the same conditions with bare electrodes. Linear sweep voltammetry (LSV) is performed at 300 rpm (rotations per minute) to investigate the electrocatalytic H_2 generation. Pt counter electrodes may be corroded under acidic conditions when large anodic potentials are applied.[63] Thus the electrocatalytic current was also measured using a glassy carbon

dx.doi.org/10.1021/cs300835a | ACS Catal. 2013, 3, 429−436

counter electrode. Very similar results were obtained (Supporting Information, Figure S1).

Detection of H_2. H_2 is generally detected by head space gas analysis by a GC fitted with appropriate detector. Such facilities are not accessible to the authors. Fontecave et.al. reported an electrochemical method for detecting H_2 using rotating ring disc electrochemistry (RRDE).[16] In an RRDE experiment a Pt-ring encircling the working EPG electrode is held at a constant potential of 0.7 V. At this potential Pt electrode oxidizes H_2, generated at the working electrode and radially diffused outward to the Pt electrode because of the hydrodynamic current produced by the rotating shaft back to H^+ generating an oxidation current. Thus a reduction current in observed in the working electrode and an oxidation current is observed in the Pt electrode. As a control experiment, in a standard three electrode cell, a Pt working electrode was held at a constant potential of 0.7 V and H_2 was introduced into the solution by gentle bubbling. The H_2 to H^+ current was immediately generated on the Pt electrode (held at a constant potential of 0.7 V), and the current persisted as long as the H_2 gas was bubbled (Figure 10). The current decayed as the H_2 gas

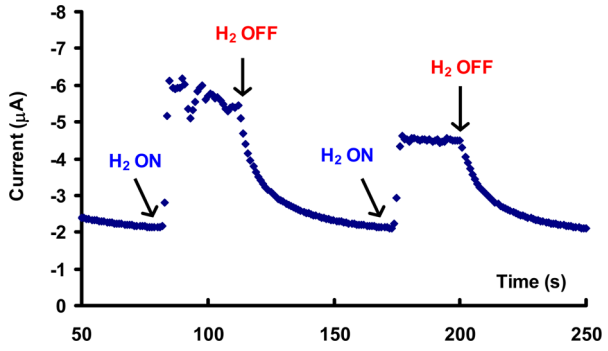

Figure 10. H_2 oxidation current on a Pt electrode held at a constant potential of 0.7 V.

bubbling was stopped. This process could be repeated several times suggesting that oxidation of H_2 back to H^+ on a Pt electrode held at a constant potential of 0.7 V is a reliable method for detecting formation of H_2 electrochemically in situ. Thus H_2 produced on the working electrodes was detected by oxidizing it back to H^+ on the Pt ring in a RRDE setup. Note that the Pt ring electrode held at 0.7 V can not reduce H^+ to H_2, that is, none of the H_2 produced can derive from Pt.

Controlled Potential Coulometry and Faradaic Yield. The controlled potential bulk coulometry experiments are performed in the same water jacket electrochemical cell that is used for the LSV. These experiments are performed in degassed 0.5 N H_2SO_4 solutions at −0.5 V vs NHE for 8 h. The shaft bearing the working electrode is rotated at 900−1100 rpm to disperse H_2 bubbles formed into the bulk solution. During electrolysis the H_2 generated was collected through an outlet of the cell and collected using an inverted buret setup. The ratio of the charge dispersed and the moles of H^+ reduced in the process (estimated from the volume of H_2 collected) is reported at the FY.

Electrolysis Using Carbon Electrodes in Domestic Batteries. The bulk electrolysis is performed using normal cheap graphite electrodes, generally used in a dry battery. The domestic graphite electrodes are extracted from Zinc−Carbon (MnO_2/NH_4Cl/Zn) dry batteries made by Nippo Pvt. Ltd. (India). These were treated with conc. HCl to get rid of any MnO_2 present. This was followed by washing with conc. HNO_3 and then with copious amounts of water. Then the electrode is dried overnight in a oven at 80 °C. Complex **A** is physisorbed on the graphite electrode by dipping it into a CH_2Cl_2 solution of the complex. Then the electrode is washed with DCM, ethanol, and water successively. The electrolysis is then performed using a Pt mesh counter electrode and a normal Ag/AgCl reference electrode.

DFT Calculations. The geometry optimizations of the complex were carried out using a 6-31g* basis set in Gaussian 03 using the BP86 functional.[64−66] The final electronic structure and energy calculations were carried out using a 6-311+g* basis set on all atoms. Frequency calculations were performed on the optimized structures to ensure a global minimum, that is, no negative frequencies. Solvation corrections were performed using a PCM model and using CH_3CN and H_2O as solvents.[67]

■ ASSOCIATED CONTENT

Ⓢ Supporting Information

Crystallographic details in CIF format. Further details are given in Figures SI-I to SI-VI as well as in discussions of the electrochemical measurements and the wave analysis. Video of profuse evolution of H_2 gas on the cathode. This material is available free of charge via the Internet at http://pubs.acs.org.

■ AUTHOR INFORMATION

Corresponding Author

*E-mail: icad@iacs.res.in (A.D.); icsgd@iacs.res.in (S.G.D.).

Notes

The authors declare no competing financial interest.

All the potential values mentioned here are with respect to NHE, but the experiments were performed using aqueous Ag/AgCl reference and corrected to NHE references.

■ ACKNOWLEDGMENTS

This research is funded by BRNS grant number 2011/36/12-BRNS/, DAE, India. S.D. acknowledges a CSIR-SRF fellowship. A.R. acknowledges the IACS-integrated Ph.D. funding. The IACS XPS facility funded by DST unit of Nano-science is gratefully acknowledged. Dr. Tushar Ghosh is gratefully acknowledged for XPS measurements.

■ REFERENCES

(1) Graetzel, M. *Acc. Chem. Res.* **1981**, *14*, 376−384.
(2) Bard, A. J.; Fox, M. A. *Acc. Chem. Res.* **1995**, *28*, 141−145.
(3) Lewis, N. S.; Nocera, D. G. *Proc. Natl. Acad. Sci. U.S.A.* **2006**, *103*, 15729−15735.
(4) Armaroli, N.; Balzani, V. *Angew. Chem., Int. Ed.* **2007**, *46*, 52−66.
(5) Cook, T. R.; Dogutan, D. K.; Reece, S. Y.; Surendranath, Y.; Teets, T. S.; Nocera, D. G. *Chem. Rev.* **2010**, *110*, 6474−6502.
(6) Turner, J. A. *Science* **2004**, *305*, 972−974.
(7) Lewis, N. S. *Science* **2007**, *315*, 798−801.
(8) Mealli, C.; Rauchfuss, T. B. *Angew. Chem., Int. Ed.* **2007**, *46*, 8942−8944.
(9) Singleton, M. L.; Bhuvanesh, N.; Reibenspies, J. H.; Darensbourg, M. Y. *Angew. Chem., Int. Ed.* **2008**, *47*, 9492−9495.
(10) Artero, V.; Chavarot-Kerlidou, M.; Fontecave, M. *Angew. Chem., Int. Ed.* **2011**, *50*, 7238−7266.
(11) Wang, M.; Chen, L.; Sun, L. *Energy Environ. Sci.* **2012**, *5*, 6763−6778.
(12) Esposito, D. V.; Hunt, S. T.; Kimmel, Y. C.; Chen, J. G. *J. Am. Chem. Soc.* **2012**, *134*, 3025−3033.

(13) Fourmond, V.; Canaguier, S.; Golly, B.; Field, M. J.; Fontecave, M.; Artero, V. *Energy Environ. Sci.* **2011**, *4*, 2417−2427.
(14) Efros, L. L.; Thorp, H. H.; Brudvig, G. W.; Crabtree, R. H. *Inorg. Chem.* **1992**, *31*, 1722−1724.
(15) Wilson, A. D.; Newell, R. H.; McNevin, M. J.; Muckerman, J. T.; Rakowski DuBois, M.; DuBois, D. L. *J. Am. Chem. Soc.* **2005**, *128*, 358−366.
(16) Le Goff, A.; Artero, V.; Jousselme, B.; Tran, P. D.; Guillet, N.; Métayé, R.; Fihri, A.; Palacin, S.; Fontecave, M. *Science* **2009**, *326*, 1384−1387.
(17) Helm, M. L.; Stewart, M. P.; Bullock, R. M.; DuBois, M. R.; DuBois, D. L. *Science* **2011**, *333*, 863−866.
(18) Tran, P. D.; Le Goff, A.; Heidkamp, J.; Jousselme, B.; Guillet, N.; Palacin, S.; Dau, H.; Fontecave, M.; Artero, V. *Angew. Chem., Int. Ed.* **2011**, *50*, 1371−1374.
(19) Connolly, P.; Espenson, J. H. *Inorg. Chem.* **1986**, *25*, 2684−2688.
(20) Baffert, C.; Artero, V.; Fontecave, M. *Inorg. Chem.* **2007**, *46*, 1817−1824.
(21) Hu, X.; Brunschwig, B. S.; Peters, J. C. *J. Am. Chem. Soc.* **2007**, *129*, 8988−8998.
(22) Jacobsen, G. M.; Yang, J. Y.; Twamley, B.; Wilson, A. D.; Bullock, R. M.; Rakowski DuBois, M.; DuBois, D. L. *Energy Environ. Sci.* **2008**, *1*, 167−174.
(23) Pantani, O.; Naskar, S.; Guillot, R.; Millet, P.; Anxolabéhère-Mallart, E.; Aukauloo, A. *Angew. Chem., Int. Ed.* **2008**, *47*, 9948−9950.
(24) Dempsey, J. L.; Brunschwig, B. S.; Winkler, J. R.; Gray, H. B. *Acc. Chem. Res.* **2009**, *42*, 1995−2004.
(25) McCrory, C. C. L.; Uyeda, C.; Peters, J. C. *J. Am. Chem. Soc.* **2012**, *134*, 3164−3170.
(26) Anxolabéhère-Mallart, E.; Costentin, C.; Fournier, M.; Nowak, S.; Robert, M.; Savéant, J.-M. *J. Am. Chem. Soc.* **2012**, *134*, 6104−6107.
(27) Sun, Y.; Bigi, J. P.; Piro, N. A.; Tang, M. L.; Long, J. R.; Chang, C. J. *J. Am. Chem. Soc.* **2011**, *133*, 9212−9215.
(28) Bernhardt, P. V.; Jones, L. A. *Inorg. Chem.* **1999**, *38*, 5086−5090.
(29) Du, P.; Knowles, K.; Eisenberg, R. *J. Am. Chem. Soc.* **2008**, *130*, 12576−12577.
(30) Lazarides, T.; McCormick, T.; Du, P.; Luo, G.; Lindley, B.; Eisenberg, R. *J. Am. Chem. Soc.* **2009**, *131*, 9192−9194.
(31) Lakadamyali, F.; Reisner, E. *Chem. Commun.* **2011**, *47*, 1695−1697.
(32) Kilgore, U. J.; Roberts, J. A. S.; Pool, D. H.; Appel, A. M.; Stewart, M. P.; DuBois, M. R.; Dougherty, W. G.; Kassel, W. S.; Bullock, R. M.; DuBois, D. L. *J. Am. Chem. Soc.* **2011**, *133*, 5861−5872.
(33) Stubbert, B. D.; Peters, J. C.; Gray, H. B. *J. Am. Chem. Soc.* **2011**, *133*, 18070−18073.
(34) Karunadasa, H. I.; Chang, C. J.; Long, J. R. *Nature* **2010**, *464*, 1329−1333.
(35) Karunadasa, H. I.; Montalvo, E.; Sun, Y.; Majda, M.; Long, J. R.; Chang, C. J. *Science* **2012**, *335*, 698−702.
(36) Quentel, F.; Passard, G.; Gloaguen, F. *Energy Environ. Sci.* **2012**, *5*, 7757−7761.
(37) Winter, M. Abundance in Earth's crust. http://www.webelements.com/periodicity/abundance_crust/
(38) USGS Commodity Statistics and Information. http://minerals.usgs.gov/minerals/pubs/commodity/
(39) Liu, T.; Chen, S.; ÓHagan, M. J.; Rakowski DuBois, M.; Bullock, R. M.; DuBois, D. L. *J. Am. Chem. Soc.* **2012**, *134*, 6257−6272.
(40) Evans, D. J.; Pickett, C. J. *Chem. Soc. Rev.* **2003**, *32*, 268−275.
(41) Vincent, K. A.; Parkin, A. *Chem. Rev.* **2007**, *107*, 4366−4413.
(42) Vignais, P. M.; Billoud, B. *Chem. Rev.* **2007**, *107*, 4206−4272.
(43) Fontecilla-Camps, J. C.; Volbeda, A.; Cavazza, C.; Nicolet, Y. *Chem. Rev.* **2007**, *107*, 4273−4303.
(44) Lambertz, C.; Leidel, N.; Havelius, K. G. V.; Noth, J.; Chernev, P.; Winkler, M.; Happe, T.; Haumann, M. *J. Biol. Chem.* **2011**, *286*, 40614−40623.
(45) Darensbourg, M. Y.; Lyon, E. J.; Zhao, X.; Georgakaki, I. P. *Proc. Natl. Acad. Sci. U.S.A.* **2003**, *100*, 3683−3688.
(46) Gloaguen, F.; Rauchfuss, T. B. *Chem. Soc. Rev.* **2009**, *38*, 100−108.
(47) Tard, C. d.; Pickett, C. J. *Chem. Rev.* **2009**, *109*, 2245−2274.
(48) Ott, S.; Borgström, M.; Kritikos, M.; Lomoth, R.; Bergquist, J.; Åkermark, B. r.; Hammarström, L.; Sun, L. *Inorg. Chem.* **2004**, *43*, 4683−4692.
(49) Cao, W.-N.; Wang, F.; Wang, H.-Y.; Chen, B.; Feng, K.; Tung, C.-H.; Wu, L.-Z. *Chem. Commun.* **2012**, *48*, 8081−8083.
(50) Le Goff, A.; Artero, V.; Metayé, R.; Moggia, F.; Jousselme, B.; Razavet, M.; Tran, P. D.; Palacin, S.; Fontecave, M. *Int. J. Hydrogen Energy* **2010**, *35*, 10790−10796.
(51) Grim, S. O.; Matienzo, L. J.; Swartz, W. E. *J. Am. Chem. Soc.* **1972**, *94*, 5116.
(52) Kumar, S. N.; Bouyssoux, G.; Gaillard, F. *Surf. Interface Anal.* **1990**, *15*, 531.
(53) Seno, M.; Tsuchiya, S. *J. Electron Spectrosc. Relat. Phenom.* **1976**, *8*, 165.
(54) Ott, S.; Kritikos, M.; Åkermark, B.; Sun, L.; Lomoth, R. *Angew. Chem., Int. Ed.* **2004**, *43*, 1006−1009.
(55) Kadish, K. M.; Frémond, L.; Ou, Z.; Shao, J.; Shi, C.; Anson, F. C.; Burdet, F.; Gros, C. P.; Barbe, J.-M.; Guilard, R. *J. Am. Chem. Soc.* **2005**, *127*, 5625−5631.
(56) Boulatov, R.; Collman, J. P.; Shiryaeva, I. M.; Sunderland, C. J. *J. Am. Chem. Soc.* **2002**, *124*, 11923−11935.
(57) Dey, A.; Jenney, F. E.; Adams, M. W. W.; Babini, E.; Takahashi, Y.; Fukuyama, K.; Hodgson, K. O.; Hedman, B.; Solomon, E. I. *Science* **2007**, *318*, 1464−1468.
(58) Fourmond, V.; Jacques, P.-A.; Fontecave, M.; Artero, V. *Inorg. Chem.* **2010**, *49*, 10338−10347.
(59) Costentin, C.; Drouet, S.; Robert, M.; Savéant, J.-M. *J. Am. Chem. Soc.* **2012**, *134*, 11235−11242.
(60) Costentin, C.; Robert, M.; Saveant, J-M *Chem. Soc. Rev.* **2013**, Advance Article , doi: 10.1039/C2CS35360A.
(61) Berben, L. A.; Peters, J. C. *Chem. Commun.* **2010**, *46*, 398−400.
(62) Stanley, J. L.; Rauchfuss, T. B.; Wilson, S. R. *Organometallics* **2007**, *26*, 1907−1911.
(63) Bockris, J. O. M.; Conway, B. E. *Trans. Farad. Soc.* **1949**, *45*, 989−999.
(64) Becke, A. D. *Phys. Rev. A* **1988**, *38*, 3098−3100.
(65) Frisch, M. J.; Trucks, G. W.; Schlegel, H. B.; Scuseria, G. E.; Robb, M. A.; Cheeseman, J. R.; Scalmani, G.; Barone, V.; Mennucci, B.; Petersson, G. A.; Nakatsuji, H.; Caricato, M.; Li, X.; Hratchian, H. P.; Izmaylov, A. F.; Bloino, J.; Zheng, G.; Sonnenberg, J. L.; Hada, M.; Ehara, M.; Toyota, K.; Fukuda, R.; Hasegawa, J.; Ishida, M.; Nakajima, T.; Honda, Y.; Kitao, O.; Nakai, H.; Vreven, T.; Montgomery, J. A.; , Jr., Peralta, J. E.; Ogliaro, F.; Bearpark, M.; Heyd, J. J.; Brothers, E.; Kudin, K. N.; Staroverov, V. N.; Kobayashi, R.; Normand, J.; Raghavachari, K.; Rendell, A.; Burant, J. C.; Iyengar, S. S.; Tomasi, J.; Cossi, M.; Rega, N.; Millam, J. M.; Klene, M.; Knox, J. E.; Cross, J. B.; Bakken, V.; Adamo, C.; Jaramillo, J.; Gomperts, R.; Stratmann, R. E.; Yazyev, O.; Austin, A. J.; Cammi, R.; Pomelli, C.; Ochterski, J. W.; Martin, R. L.; Morokuma, K.; Zakrzewski, V. G.; Voth, G. A.; Salvador, P.; Dannenberg, J. J.; Dapprich, S.; Daniels, A. D.; Ö. Farkas, Foresman, J. B.; Ortiz, J. V.; Cioslowski, J.; Fox, D. J. *Gaussian 03*, C.02; Gaussian, Inc.: Wallingford, CT, 2004.
(66) Perdew, J. P. *Phys. Rev. B* **1986**, *33*, 8822−8824.
(67) Miertus, S.; Scrocco, E.; Tomasi, J. *Chem. Phys.* **1981**, *55*, 117−129.